



# Extracting the Planckian scattering rate of the Strange Metal $\text{PdCrO}_2$ from Angular-Dependent Magneto-Resistance Measurements

Juan L. Santana González

Under supervision of **Gaël Grissonnanche**

Realized in  
**Laboratoire des Solides Irradiés**

A thesis submitted in partial fulfillment of the requirements for the degree:  
**International Centre for Fundamental Physics MSc program**

Paris, 24<sup>th</sup> June 2024



| PSL

**quantum**  
PARIS-SACLAY

## Abstract

Strange Metals are one of biggest mysteries in Condensed Matter Physics in the 21<sup>st</sup> century. The simple observation of a linear dependence with temperature in the resistivity of some strongly-correlated materials seems to imply the breakdown of the quasiparticle picture and a new quantum limit for inelastic scattering and dissipation. The consequence is that, in this (Planckian) limit, electrons interact with a rate  $\hbar/\tau = k_B T$ , the fastest allowed by quantum mechanics. Interestingly, these materials seem to be linked with unconventional conductivity in ways we still do not understand. During my M2 internship at the *Laboratoire des Solides Irradiés*, I joined a team of experts with the objective of uncovering the connections between antiferromagnetic fluctuations, the strange metal phase and the emergence of unconventional superconductivity. To this end, we measured c-axis bulk resistivity under extreme magnetic fields in the strange-metal PdCrO<sub>2</sub> and its isostructural compound PdCoO<sub>2</sub>, with the objective of extracting the scattering rate directly from observations using Angle-Dependent MagnetoResistance (ADMR) techniques and semiclassical considerations. PdCrO<sub>2</sub> is a frustrated antiferromagnet down to its Néel temperature of 37.5K. Above such temperature, it displays perfectly linear resistivity, which has been observed to be consistent with Planckian scattering. The antiferromagnetic fluctuations are believed to be the cause of the linear resistivity. PdCoO<sub>2</sub> is isostructural to PdCrO<sub>2</sub> but non-magnetic, and shows the  $T^2$  behaviour in resistivity expected for conventional metals. Furthermore electron-phonon scattering has been measured to be very weak in this family of materials. With ADMR, we will be able to extract the Fermi surface and the scattering time  $\tau(\mathbf{k}, T)$  simultaneously in both materials. A direct comparison in the same conditions will allow us to draw conclusions on the role that antiferromagnetic fluctuations play at reaching the Planckian limit.

# Contents

<b>1</b>	<b>Introduction: The Strange Metal phase and the Planckian limit</b>	<b>1</b>
1.1	The Strange Metal . . . . .	1
1.2	The Planckian limit of the scattering rate . . . . .	3
1.3	Connection with unconventional superconductivity and antiferromagnetism . . . . .	5
<b>2</b>	<b>Materials: The isostructural delafossites PdCrO<sub>2</sub> and PdCoO<sub>2</sub></b>	<b>6</b>
2.1	Motivation: why delafossites? . . . . .	6
2.2	Band Structure . . . . .	7
<b>3</b>	<b>Method: Angle-Dependent MagnetoResistance and Chamber's formula</b>	<b>9</b>
3.1	Angle-Dependent Magnetoresistance oscillations . . . . .	9
3.2	Boltzmann semiclassical transport and the Chamber's formula . . . . .	10
<b>4</b>	<b>Measurement: ADMR in extreme magnetic fields</b>	<b>12</b>
4.1	Preparation of the samples . . . . .	13
4.2	Performing the experiment under extreme magnetic fields . . . . .	14
<b>5</b>	<b>Results</b>	<b>15</b>
5.1	Results of the measurements at the NHMFL . . . . .	15
5.2	Preliminar simulations for PdCoO <sub>2</sub> . . . . .	17
<b>6</b>	<b>Conclusion</b>	<b>19</b>
<b>A</b>	<b>Extended Figures of the measurements at the NHMFL</b>	<b>26</b>
<b>B</b>	<b>Simulations in Nickelates</b>	<b>28</b>

# 1 Introduction: The Strange Metal phase and the Planckian limit

The concept of a metal is now natural to us. Blatantly, we call metallic systems those in which charge carriers (particles that carry charge) are able to move through certain distances before they scatter. Due to the nature of the crystalline potential created by the atomic lattice, the momentum of the electrons of the material is quantized. Pauli's exclusion principle dictates that two electrons cannot occupy the same quantum state, so the electrons will fill the available momentum states up to the so-called Fermi energy. In the absence of perturbation, there exist then a collection of momentum states forming a constant-energy surface in momentum space, called the Fermi surface (FS), which contains the last occupied states with energy equal to this Fermi energy. When an external electric field  $\mathbf{E}$  is applied, the FS is displaced in the direction of the field, as a consequence of the Lorentz force. An imbalance will occur between different momentum states and the average momentum of the electrons will become nonzero, giving rise to an electrical current.

The picture is thus simple and well understood for "conventional" metals, one of the biggest successes of the field of Condensed Matter physics in the 20<sup>th</sup> century. However, during the last 30 years, new evidence has been showing that the physics of electric transport may not be as simple as it seems. In this text I present one of the most intriguing types of conducting materials, the so-called *Strange Metals*. I will try to motivate the interest of their study and their uniqueness, and which approach we have chosen to understand them better.

## 1.1 The Strange Metal

In families of unconventional superconductors like cuprates[1–3], iron-based superconductors[4] or heavy-fermions[5], experimental observations show that their resistivity has a linear dependence on temperature before the critical temperature in which they become superconductors. Moreover, it does not saturate at any temperature, in contrast to what is seen in conventional metals. These seemingly naive differences hide much deeper consequences[6]. The absence of saturation, as well as the absence of a noticeable change in the slope of the T-linear curve at any temperature, indicates that similar physics is present for the entire energy range. The system is then said to be *energy-scale invariant*. Scale invariance in quantum systems is usually related to a Quantum Critical Point (QCP) separating two phases at zero temperature, as it is indeed the case for most of materials presenting the strange metal phase[5, 7, 8]. Another important reason for the interest in strange metals is that they seem to be intimately connected with unconventional superconductivity. Indeed, many materials with really different properties (see for example Fig.2, where I present the T-linear behaviour in materials with quasi-1D, 2D, quasi-2D and 3D character) are linked together by this strange behaviour, and by the existence of unconventional superconductivity.

In model metallic systems, electrons do not interact with each other. They are subject to a periodic potential that shapes their energy, but once they are excited over the Fermi energy, they are well defined single particles. The only reason for them to return back to the ground state energy is scattering or interaction with external fields. In real materials, Coulomb interaction is present between electrons and the picture changes slightly. Upon interaction, electrons no longer compose the excitation of the system. In the language of

quantum mechanics it is said that they are no longer eigenstates of the system. Therefore, electronic states on the Fermi Surface are no longer stationary, and the electron itself (apart from an energy renormalization) acquires a finite lifetime

This lifetime  $\tau$ , produced by the electron-electron interaction, affects directly the transport in the system. Due to Pauli's exclusion principle, two electrons can scatter only if their energy states lie within a shell of width  $k_B T$  around the Fermi energy  $\varepsilon_f$ . Furthermore, due to energy conservation, their final state must also lie in this shell, where there are unoccupied states. For an electron with a given energy, the probability of the process, also known as scattering rate  $\Gamma = 1/\tau$ , is given by the "amount of options" (or volume of the phase space) one has when choosing which second electron it scatters with. Since one energy is fixed by energy conservation, this "amount of options" scales as  $\sim (k_B T)^2$ . There are precisely these electrons, close to the Fermi surface, which contribute to conduction, hence one expects the relevant relaxation time for transport to have also the form  $1/\tau \sim (k_B T)^2/\hbar$ , leading to the resistivity scaling as  $\rho \sim T^2$

Therefore, electron-electron interaction as explained by Fermi Liquid theory cannot account for the observed T-linear resistivity<sup>1</sup>. Could it be phonons behind it? Indeed electron-phonon scattering is dominant at high temperatures and it is known to produce T-linear resistivity in conventional metals. The absence of saturation at high temperature is also observed in some elemental metals like Copper or Gold. The real surprising fact is that this T-linear behaviour extends all the way down to 0 temperature, where phonons are frozen and cannot contribute to scattering. Therefore the T-linear resistivity cannot be explained by electron-phonon scattering.

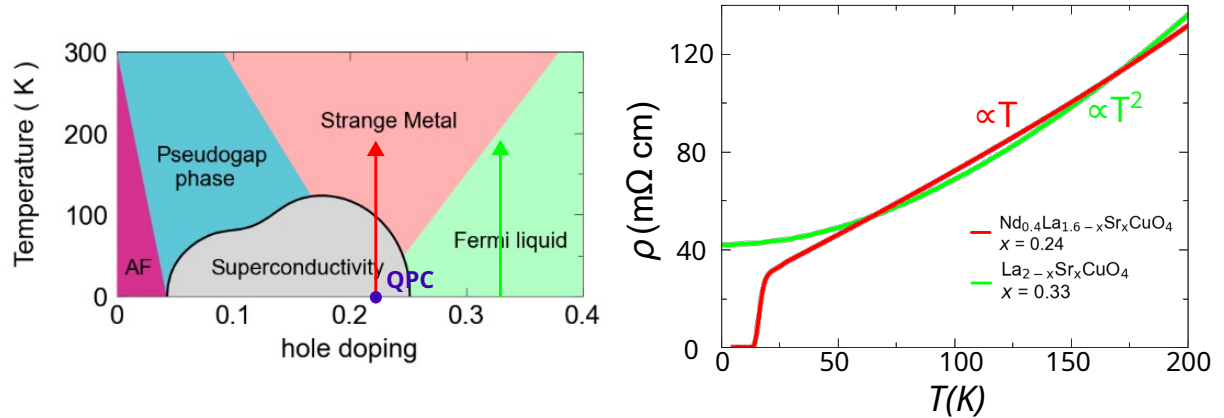


**Figure 1: Conventional metal vs Strange Metal.** (Left) Schematic phase diagram of cuprates. Cuprates show an extended strange metal phase arising from the quantum critical point (QCP) that separates the Fermi Liquid regime from the Pseudogap regime. This is the same regime where unconventional superconductivity arises. Colored arrows indicate the regions where the resistivity measurements of the right were performed. (Right) T-linear and T-squared resistivity generally observed in cuprates. When quadratic dependence is observed, the system behaves like a normal metal, while when there is linear dependence, there is also superconductivity. Data adapted from ref.[1](red curve) and[9](green curve).

<sup>1</sup>This does not mean however, that some other kind of strongly-correlated electron-electron scattering is behind the strange metal behaviour. This question is precisely at the heart of present investigations.

Surprisingly, the slope of the T-linear resistivity does not change over the complete range of temperatures in which  $\rho(T)$  is linear, a range that can be extremely wide, expanding up to 4 orders of magnitude in the hole-doped cuprates for example. A non-stagnating resistivity (i.e. scattering rate) at  $T \rightarrow 0$  therefore has no explanation if the charge is carried by particles. This would imply a breakdown of the quasiparticle picture *at all temperatures*. Charge would be carried in these systems by some kind of nonlocal highly-entangled many-body state, which has not been identified yet. Strong correlations seem to induce a scattering rate that is not well understood by the usual means of the theory of metals, and that gives rise to the anomalous resistivity. The first approach to understand better this physics is to study the scattering rate itself, which will be our main objective. This brings us back to the concept of scale invariance in these systems, and inevitably, to the Planckian limit.

## 1.2 The Planckian limit of the scattering rate

An even more astonishing property of strange metals is their connection to the Planckian time. In analogy with the Planckian scale, which is said to be smallest lengthscale allowed by quantum mechanics<sup>2</sup>, one can define a Planckian time as the smallest possible timescale in which any dynamics can occur<sup>3</sup>. In the context of Condensed Matter Physics, in which the energy scale of the environment is set by temperature, its definition takes the form:

$$\tau_P \equiv \frac{\hbar}{k_B T}$$

As we have seen, resistivity seems to follow the law  $\rho = \rho_0 + AT$ , in which  $\rho_0$  is some residual resistivity related to the elastic scattering with impurities and is T-independent. The coefficient A indeed varies from one material to another. However, it hides a universal property that links all of them. Take cuprates, the easier example having a single band and in which T-linear resistivity is most extensively observed. If one considers the simple Drude formula,  $\rho = m^*/ne^2\tau$ , then  $A = (m^*/ne^2)(1/\tau)(1/T)$ . Here  $m^*$  is the effective mass,  $n$  the charge carrier density and  $e$  the electron charge. What is usually done in experiments is to consider, within this simple semiclassical formalism, that the scattering rate is proportional to the Planckian bound:  $\hbar/\tau = \alpha k_B T$ . Substituting, one then finds that:  $A/d = \alpha(h/2e^2)1/T_F$ . Here,  $d$  is the average interlayer spacing and  $T_F = (\pi\hbar^2/k_B)/(nd/m^*)$  is the Fermi temperature. These are two unique material-dependent quantities, which can be known from quantum oscillations or specific heat measurements for example. The final step is to calculate  $\alpha$  from the measured slope of the resistivity and the material parameters. In the majority of unconventional superconductors,  $\alpha$  is found to be  $\sim 1$  within experimental errorbars (see Table1). This is the way strange metals have been found to follow the Planckian bound so far. One should say that some deviations may be expected since Drude's formalism is not supposed to hold in strongly-correlated systems (actually, what is really surprising is that it

---

<sup>2</sup>The Planckian scale makes its apparition in the context of quantum gravity, in which it defines the length scale below which a quantum gravity theory takes over the classical version:  $l_P = \sqrt{\hbar G/c^3}$ . This is the origin of the links between strange metal behaviour and quantum gravity that have been discussed by the community[6, 10, 11]. This topic is subject of intense discussion and, as exciting as it seems to me, it will not be discussed in this report.

<sup>3</sup>To see why, consider an argument based on the uncertainty principle  $\tau\Delta\varepsilon \gtrsim \hbar$ . If  $\tau < \hbar/k_B T$  then  $\Delta\varepsilon \gtrsim k_B T$ , meaning the energy spread is wider than the thermal energy itself. This means charge carriers no longer have a well-defined energy or momentum, and the whole Fermi surface picture breaks down. For the single-particle case the argument is solid, but one should be more caution when treating many-body systems. Indeed the limit also holds but the argument is more complex, I direct the interested reader to ref.[12].

Table 1: **Slope of  $T$ -linear resistivity versus Planckian limit in several materials.** Adapted from ref.[13]

Material	$n$ ( $10^{27}$ m $^{-3}$ )	$m^*$ ( $m_e$ )	$A/d$ ( $\Omega$ K $^{-1}$ )	$h/(2e^2 T_F)$ ( $\Omega$ K $^{-1}$ )	$\alpha$
Bi2212	6.8	$8.4 \pm 1.6$	$8.0 \pm 0.9$	$7.4 \pm 1.4$	$1.1 \pm 0.3$
Bi2201	3.5	$7 \pm 1.5$	$8 \pm 2$	$8 \pm 2$	$1.0 \pm 0.4$
LSCO	7.8	$9.8 \pm 1.7$	$8.2 \pm 1.0$	$8.9 \pm 1.8$	$0.9 \pm 0.3$
Nd-LSCO	7.9	$12 \pm 4$	$7.4 \pm 0.8$	$10.6 \pm 3.7$	$0.7 \pm 0.4$
PCCO	8.8	$2.4 \pm 0.1$	$1.7 \pm 0.3$	$2.1 \pm 0.1$	$0.8 \pm 0.2$
LCCO	9.0	$3.0 \pm 0.3$	$3.0 \pm 0.45$	$2.6 \pm 0.3$	$1.2 \pm 0.3$
(TMTSF) $_2$ PF $_6$	1.4	$1.15 \pm 0.2$	$2.8 \pm 0.3$	$2.8 \pm 0.4$	$1.0 \pm 0.3$

does). One of the main objectives we have with the experiment that we will perform is to extract the scattering rate without almost any approximation, hence providing much stronger evidence than those based in Drude's formula.

Let me stress another puzzling consequence of this bound for the scattering rate. In general, the scattering rate of any material can be expressed as the sum between an elastic term, in which electrons conserve their energy upon scattering, and an inelastic term, in which there is energy exchange. An important concept to note is that the Planckian limit only affects inelastic scattering. One can see this for example considering the elastic scattering with impurities inside a material. Even when  $T \rightarrow 0$ , there is still residual resistivity due this scattering process, because Bloch electrons are delocalized over the whole material. In other words, electrons suffer this scattering due to not being eigenstates of the system, and not because of many body interactions[12]. However in this regime  $1/\tau_P \rightarrow 0$  and so elastic scattering is not subject to Planckian limit. Hence, only the inelastic part of the scattering rate follows the Planckian limit, which inevitably establishes a connection with dissipation. This connection seems to set a quantum mechanical limit for the energy dissipation within a system, rising from the strong many-body interactions. This bound would have deep connections with not-understood topics like quantum many-body thermal relaxation or bounds of many-body quantum dynamics[12], and would in principle be explorable in these novel quantum materials, although no certainties can be obtained yet from theory.

Finally, this timescale has also been connected with quantum criticality in the past[18, 19], and has been observed to dominate the dynamics in unconventional superconductors via many different techniques like photoemission[20], optical conductivity[21] or dc transport[21]. It has also been shown to arise in quantum critical antiferromagnets by explicit calculations[22, 23], another phase present in multiple unconventional superconductors. Another reason for the connection between strange metals and quantum criticality is that the strange metal phase always shows up in systems with QCP's. However, in many systems like overdoped (hole and electron) cuprates (see Fig.1) or Bechgaard salts[24], the strange metal behaviour appears over a whole extended region of the phase diagram, and not only on a certain point defining a QCP. This is unexpected from a system displaying quantum criticality and has to be included to the list of mysteries related to the strange metals. As a summary, understanding the emergence of this scattering rate could shine light not only on the elusive origin of unconventional superconductivity, but also on other quantum many-body problems.

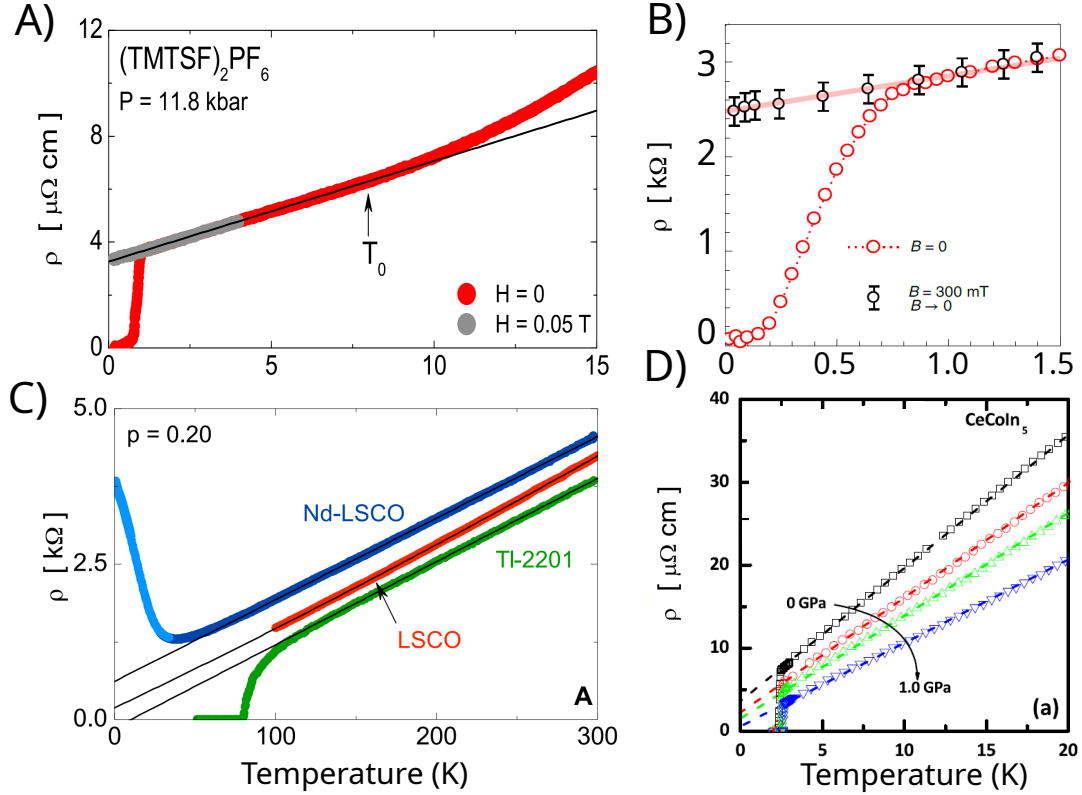


Figure 2: **T-linear resistivity in systems of different nature.** (A) The quasi-1D Bechgaard salt  $(\text{TMTSF})_2\text{PF}_6$ . Adapted from ref.[4]. (B) T-linear resistivity in magic-angle twisted bilayer graphene. Adapted from ref.[14]. (C) T-linear resistivity in different hole-doped cuprates. Adapted from refs.[15](red curve),[16](blue curve) and [1](green curve). (D) T-linear resistivity in the heavy-fermion superconductor  $\text{CeCoIn}_5$  for different pressures. Adapted from ref.[17].

### 1.3 Connection with unconventional superconductivity and antiferromagnetism

In many different unconventional superconductors[25, 26] an empirical law is observed that relates the superfluid density of the superconducting state  $n_s$  with the critical temperature  $T_c$  via the normal-state conductivity  $\sigma(T_c)$ :  $n_s \propto \sigma(T_c)T_c$ . Turns out that this relation holds only if the relaxation time related to the conductivity (in a semiclassical framework) is precisely the Planckian time  $\tau_P$ . In other words, and coming back to the concept of dissipation, unconventional superconductors seem to be those materials whose normal state dissipates energy as fast as allowed by quantum mechanics[26]. Moreover, strange-metal behaviour and superconductivity have been found to appear together in the phase diagram in cuprates[25], Bechgaard salts[4], the recently-discovered nickelates[27] and magic-angle twisted bilayer graphene[14, 28].

Another important concept is present in the universal behaviour of unconventional superconductors: magnetism[29]. Antiferromagnetism (AFM) is present in most of unconventional superconductors despite of their structure or dimensionality. Indeed, it has been conjectured that antiferromagnetic fluctuations appearing near a QCP can give rise to the pairing of electrons which results in the superconducting state[30–33]. This connection makes apparent that AFM fluctuations also play an important role in the emergence of the strange metal.

In conclusion, one seems to end up with more questions the more one investigates. Is the strange-metal the underlying ground state of unconventional superconductivity, once it has been suppressed? What is the connection between the Planckian limit of the scattering rate and antiferromagnetic fluctuations? These are precisely the questions we aimed to answer with the experiment carried out during my internship at the Laboratoire des Solides Irradiés, École Polytechnique. We wanted to perform the most pristine comparison possible between two materials whose only difference is the presence of antiferromagnetic fluctuations, but that nonetheless show very different behaviour, one is a conventional metal and the other is stranger. I present these materials in the next section, while our experimental approach is explained in sections 3 and 4. In section 5, I will focus on our results and initial observations, and finally I will conclude in section 6 with a description of the (many) things still left to understand during my PhD project.

## 2 Materials: The isostructural delafossites $\text{PdCrO}_2$ and $\text{PdCoO}_2$

Delafossites are quasi 2D materials with chemical formula  $\text{ABO}_2$ , formed by layers of highly conductive elements like Pd, Ag or Pt (A), intercalated by diverse oxides, like Co, Cr, Fe, Al or Ga (B). On the interlayer direction, the layers are arranged in ABC fashion, with all layers having triangular structure. These materials can have very diverse properties depending on their exact composition, like being metallic or semiconducting, or having a well defined magnetic moment[34]. In our case, we will focus in the metallic delafossites  $\text{PdCoO}_2$  and  $\text{PdCrO}_2$ .

### 2.1 Motivation: why delafossites?

$\text{PdCrO}_2$  is a magnetic metal, with a non-zero magnetic moment in its  $\text{CrO}_2$  layers, and presents a frustrated antiferromagnetic (AFM) phase below its Néel temperature of 37.5K. Due to the geometric frustration of the triangular  $\text{CrO}_2$  layer, the material is expected to maintain AFM fluctuations during a large range of temperatures. Below this temperature, it has been observed to undergo magnetic reconstruction of its Fermi Surface<sup>4</sup>[35]. More importantly for us,  $\text{PdCrO}_2$  shows T-linear in-plane resistivity from 100K all the way up to room temperature, whose scattering rate has been reported to reach the Planckian limit[36]. Therefore,  $\text{PdCrO}_2$  has the essential ingredients to be a strange metal

On the other hand,  $\text{PdCoO}_2$ , its non-magnetic isostructural compound, is one of the most conductive oxides ever found, with an electronic mean free path of  $\sim 20\mu\text{m}$  under 10K[37]. Its in plane resistivity shows a strong  $T^2$  component at low temperature, signature of conventional metals. Furthermore, theoretical calculations have shown a remarkably low electron-phonon coupling in this material[38]. This fact and the absence of T-linear resistivity in  $\text{PdCoO}_2$  are our main arguments to believe that the T-linear resistivity of  $\text{PdCrO}_2$  is due to strange-metal physics, and not simple electron-phonon scattering at high temperature.

These materials hold interesting physics by themselves, and there are three main reasons that make them a great platform to study the origin of the strange metal physics:

---

<sup>4</sup>It is worth mentioning that the fields used for the quantum oscillation measurement in this study were quite lower than in our case. We could in principle expect a magnetic breakdown and therefore recovery of the original Fermi surface at high fields.

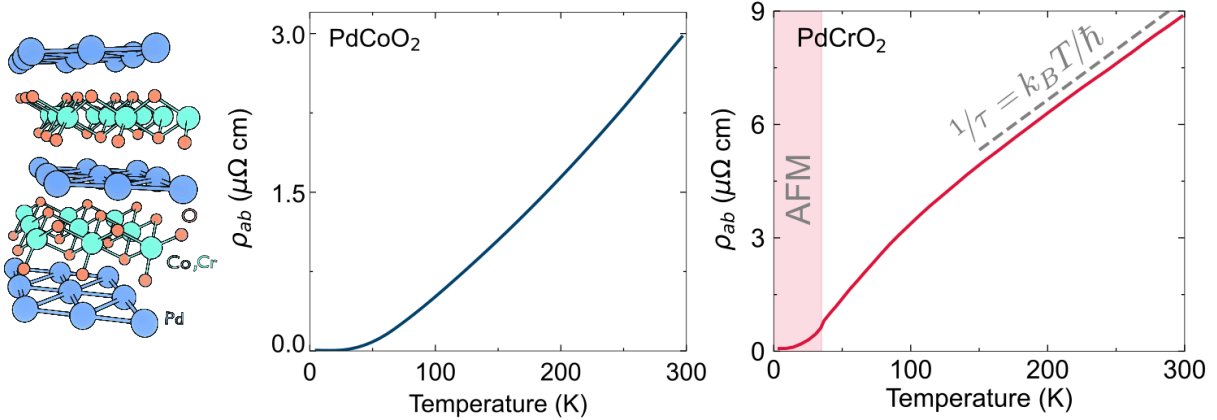


Figure 3: Structure of the delafossites and in-plane resistivity of  $\text{PdCoO}_2$  (**left**) and  $\text{PdCrO}_2$  (**right**), data taken from refs[37] and[36].

- They have a remarkably simple dispersion. A single band with Pd character crosses the Fermi level in both materials, as shown from ARPES[39, 40] and confirmed by DFT+DMFT calculations[41].
- These are extremely clean materials. In fact, the question of why are they so clean is a complete research question by itself. Essentially, the impurities are “pushed away” towards the oxide layers, resulting in an extremely clean and conducting Pd layers[42]. As an example, one can compare the residual resistivity of  $\text{PdCoO}_2$  of  $\sim 7\text{n}\Omega/\text{cm}$ [37, 43] with that of ultrapure copper, of  $\sim 0.2\text{n}\Omega$ [44].
- They are completely isostructural, both in coordination and structure. Moreover, several ARPES measurements[39, 40] and quantum oscillation experiments[35, 37] show an almost identical Fermi Surface (above  $T_{\text{Neel}}$ ), which has been confirmed by DFT and DMFT calculations[41] (see section 2.2).

These properties are precious to us because they allow for direct comparison between two almost-identical systems whose sole difference is the presence of an antiferromagnetic phase, which in principle must be the reason for the presence (and absence) of strange metal behaviour. The importance of the two first points is that they allow us to make electrical transport experiments, and they make the analysis simple enough. A simple dispersion can be modeled using a single-band Tight Binding (TB) model, while in a clean material transport is dominated by the scattering channels of interest, which are electron-electron and electron-phonon scattering. Our objective will then be to extract simultaneously and directly the scattering rate, which we expect to be the only parameter producing the stark difference in the data by the argument of point three. I will motivate how do we plan to do this and why in the next section.

## 2.2 Band Structure

To further motivate the similarities between both materials, I direct the reader’s attention to Figs.3 and 4. In them, we can see the conventional cell, band dispersion and the Fermi surface (FS) in the  $k_x$  and  $k_y$  plane, whose similarity is contrasted with the difference in resistivity. The bands and the FS have been calculated using Density Functional Theory (DFT) and Dynamical Mean Field Theory (DMFT) as explained in [41].

In terms of Fermi surface both materials are remarkably similar. ARPES finds similar results[39, 40] with slight deviations like more rounded corners of the hexagonal shape. Since we will do bulk transport experiments, the most reliable comparison with our findings will be with quantum oscillations measurements, which also has shown evidence of a great resemblance between the complete 3D Fermi surfaces of both materials[35, 37] above the antiferromagnetic transition of PdCrO<sub>2</sub>.

Following the discussion with the support of all the methods already mentioned, both materials show a single band crossing the Fermi energy. This band has a very strong Pd character, with no contribution of the oxide planes in PdCoO<sub>2</sub>. In PdCrO<sub>2</sub> DFT shows a mixed Pd-Cr band, however the Chromium energy levels are displaced by correlations above the Fermi energy once included in the DMFT calculation, resulting in a Pd band. For this reason, we are able to describe the complete dispersion with a single-band Tight Binding model, by taking into consideration only the hopping integrals of the Pd atoms. This was part of my work at the beginning of my internship, as well as comparing that the resulting Fermi surface matches with the expectations. The necessity of this Tight Binding model will become clear in the next section:

$$\begin{aligned} \varepsilon(\mathbf{k}) = & t(\cos(ak_y) + \cos(\frac{\sqrt{3}}{2}ak_x - ak_y/2) + \cos(\frac{\sqrt{3}}{2}ak_x + ak_y/2)) + \\ & t'(\cos(\sqrt{3}ak_x) + \cos(\frac{\sqrt{3}}{2}ak_x - \frac{3}{2}ak_y) + \cos(\frac{\sqrt{3}}{2}ak_x + \frac{3}{2}ak_y/2)) + \\ & t''(\cos(2ak_y) + \cos(\sqrt{3}ak_x - ak_y) + \cos(\sqrt{3}ak_x + ak_y)) + \\ & t_z(\cos(\frac{\sqrt{3}}{3}ak_x + ck_z/3) + \cos(-\frac{\sqrt{3}}{6}ak_x + ak_y/2 + ck_z/3) + \cos(\frac{\sqrt{3}}{6}ak_x + ak_y/2 - ck_z/3)) \end{aligned}$$

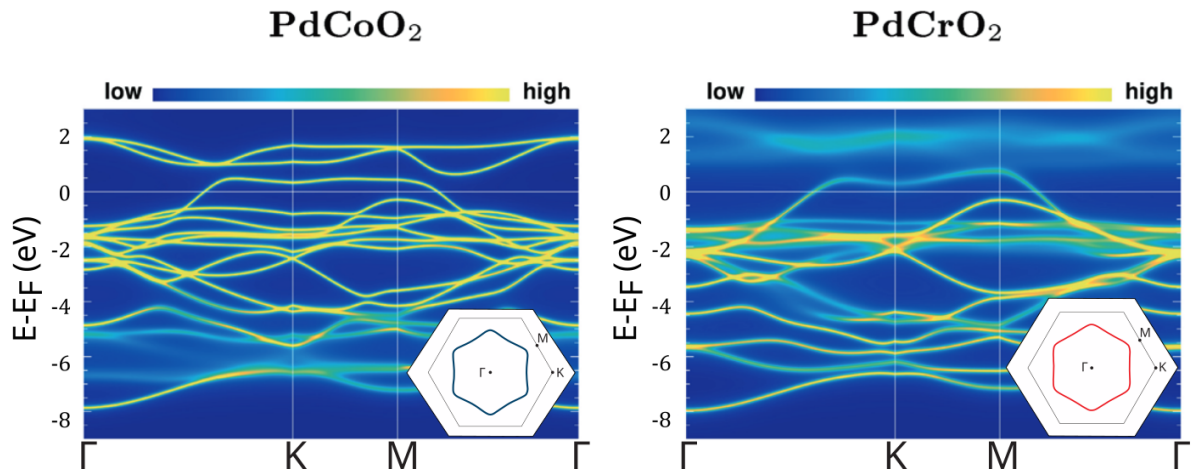


**Figure 4: DFT+DMFT calculations for the band structure of both delafossites.** A single band crosses the Fermi energy, located at 0 in this scale. This will be our region of interest. Insets show the calculated 2D Fermi surface. I stress the great similarities between them, both in structure and dispersion. Adapted from ref.[41].

### 3 Method: Angle-Dependent MagnetoResistance and Chamber's formula

The mysterious Planckian scattering rate seem to play a central role in the physics of strange metals. With the presented materials, we want to extract such scattering rate to make a direct comparison. Due to the cleanliness, the single-band character and the quasi-2D character of the delafossites, they represent the perfect candidate to perform Angle-Dependent MagnetoResistance (ADMR). This method is based on the oscillations that appear in the resistivity of some materials when a magnetic field is applied and its orientation with respect to the unit cell vectors is varied. We perform bulk transport experiments in a 4-point contact configuration, sending a current and measuring a voltage (see scheme in Fig.5) along the c-axis, to extract the resistivity. We do so under extreme magnetic fields to enhance the magnetoresistance oscillations, and along the inter-plane direction where the strong electronic correlations are present. Finally, these oscillations are fitted through simulations of the semiclassical Boltzmann transport theory. The location, amplitud and frequency of these oscillations contain all information necessary to extract the complete Fermi surface and, more importanly, the electronic scattering rate (momentum and temperature dependence included). This advanced technique has already proved useful to extract important information in quantum materials[45–47] including delafossites.

#### 3.1 Angle-Dependent Magnetoresistance oscillations

When a magnetic field  $\mathbf{B}$  is applied to a metal, electrons with the ability to move will feel the Lorentz force and try to describe circular orbits. Since they have a well defined momentum distribution, the Fermi surface, they will follow paths in momentum space embedded in this surface. Therefore, the orbits are directly dependent on the topography of the Fermi surface. The initial question to understand ADMR is, how can the Lorentz force affect transport?

Suppose we apply an electrical field  $\mathbf{E}$  to the material. The conductivity  $\sigma$  is defined (in semiclassical means) as the relation between  $\mathbf{E}$  and the created current density  $\mathbf{J}$ . In general,  $\sigma$  is a tensor, since current and applied field need not to be parallel. If  $\mathbf{B}$  is also applied, the mentioned orbits appear, and the velocity of the electrons will be modified. This will have important consequences for the conductivity  $\sigma$ , for example giving rise to out-of-diagonal components (Hall effect). Since conductivity is in general very complicated to measure in bulk transport experiments, we are interested here in its inverse value, the resistivity  $\hat{\rho} = \hat{\sigma}^{-1}$ , which will show related behaviour. As the orbits depend on the topography of the FS, and are always described in planes perpendicular to the magnetic field, varying the orientation of the field will produce different types of orbits, which will average the velocities of electrons in different ways, and therefore modify the resistance value. The “extra” resistance that appears due to this effect is called *magneto-resistance*. Our technique is based on varying the orientation of the magnetic field while maintaining its amplitud constant, and measuring such magneto-resistance, hence *Angle-Dependent Magneto-Resistance* or ADMR.

I still have not mentioned what is the role of the scattering rate  $1/\tau$  in our technique. When the electrons perform orbits, they do so with a characteristic frequency called the cyclotron frequency  $\omega_c = e/m^*B$ , where  $e$  is the electron charge,  $m^*$  its mass and  $B$  the mag-

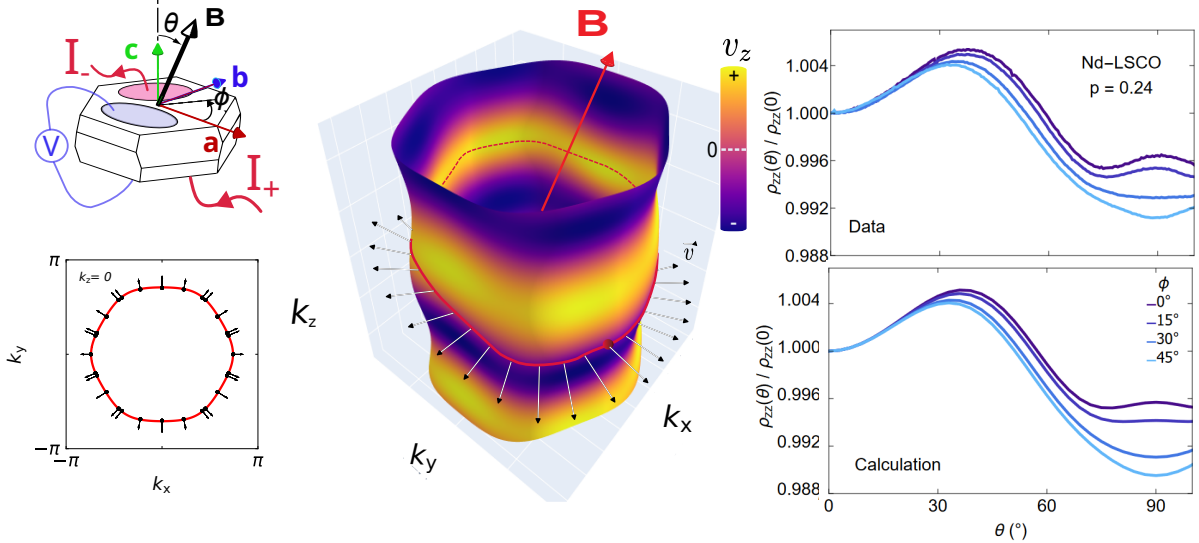


Figure 5: **Angle-Dependent MagnetoResistance schemes and experimental results.** (Left) Scheme of the c-axis resistivity measurements with the 4-point measurement configuration (see section 4.1). Axis correspond to the crystallographic basis. Below it, the 2D Fermi surface of  $\text{PdCoO}_2$  is shown at  $k_z = 0$ , with arrows denoting the velocity at each point of the surface. (Center) 3D Fermi surface of  $\text{PdCoO}_2$ . Corrugations in the  $k_z$  direction are exaggerated for visualization. Arrows show the velocities along the orbit. (Right) Example of ADMR measurement and successful simulation using semiclassical transport with our home-made algorithms, adapted from ref.[48]

nitude of the magnetic field<sup>5</sup>. During the orbit, the electron will still be scattered within a characteristic timescale  $\tau$ . There is then a competition between how fast can an electron complete a closed orbit and how long it lives. If  $\omega_c \tau \gg 1$ , electrons that describe closed orbits will return to their initial states many times before being scattered. Since transport depends on the average velocity of all electrons following this orbit, the velocities in the plane of orbit will be averaged to zero. The consequence is a sudden decrease in conductivity and a peak in resistivity at the given orientation of  $\mathbf{B}$ . Another possibility is that the orbit is open, and in such case no averaging occurs.

Therefore, if one is able to measure the oscillations of magnetoresistance at sufficiently high fields, for a complete set of angles, one can extract information about the Fermi surface topography (given by the shape of the curve) and the scattering rate (given the prominence and location of the oscillations for a known magnetic field) at the same time, and directly from experiments. However, the analysis of these curves cannot be done in general just by looking at them. It is necessary that we perform simulations of the ADMR curves for different scattering rates until the simulation resembles the data, and finally fit to the results of the experiment to obtain the desired information.

### 3.2 Boltzmann semiclassical transport and the Chamber's formula

The semiclassical framework for transport has delivered very good results even in quantum materials due to the quasiparticle picture. It can furthermore be related to a more complicated Green's function-based formalism, which we will not be following in this report[49, 50].

<sup>5</sup>There is a subtlety here in that  $m^*$  is not really the regular band mass as defined by the dispersion. Indeed, the characteristic mass in the quasiparticles that participate in transport is rather given by the Fermi velocity  $v_f$  and Fermi momentum  $k_f$ , hence in this case  $m^* = \hbar k_f / v_f$ .

However, it can still be very useful to take a look at the basics of semiclassical formalism to understand what we can learn from an ADMR measurement.

First of all, the electrons of a metal are influenced by the magnetic field  $\mathbf{B}$  via the Lorentz force, producing an orbit given by the classical equation:

$$\hbar \dot{\mathbf{k}} = -e(\mathbf{E} + \mathbf{v}(\mathbf{k}) \times \mathbf{B}) \quad (1)$$

$$\mathbf{v}(\mathbf{k}) = \frac{1}{\hbar} \nabla_{\mathbf{k}} \varepsilon(\mathbf{k}) \quad (2)$$

Here,  $\mathbf{k}$  is the crystalline momentum of the electron, and it is limited to the Fermi surface<sup>6</sup>. The velocity  $\mathbf{v}$  follows the usual definition in materials, and is directly related to the band dispersion  $\varepsilon(\mathbf{k})$ . This is a non-linear equation, since the velocity changes at every point of the orbit following the topography of the Fermi surface.

In presence of external fields, the distribution function for the occupation of states itself  $f(\mathbf{k}(t))$  is perturbed, which is the most important idea of the semiclassical framework. In a first approximation, we can consider that the properties of transport are mainly governed by a single timescale  $\tau(\mathbf{k}, T)$ , called relaxation time, which is precisely the scattering time we have been talking about. Under this consideration, the system relaxes in absence of perturbation towards the Fermi-Dirac distribution function  $f_0(\varepsilon_{\mathbf{k}}) = (1 + e^{(\varepsilon_{\mathbf{k}} - \mu)/k_B T})^{-1}$ . For the time evolution of the out of equilibrium state  $f(\varepsilon_{\mathbf{k}})$  this means:

$$\frac{d}{dt} f(\mathbf{k}(t)) = \frac{f_0(\mathbf{k}(t)) - f(\mathbf{k}(t))}{\tau(\mathbf{k}(t))} \quad (3)$$

$$\implies f(\mathbf{k}(t)) = f_0(\mathbf{k}(t)) - \int_{-\infty}^t dt' \frac{df_0(\varepsilon_{\mathbf{k}(t')})}{dt'} \exp(-\int_{t'}^t dt''/\tau(\mathbf{k}(t''))) \quad (4)$$

This is the so-called *relaxation time approximation*, and it is the only major approximation we consider in our theoretical analysis. There are many excellent examples of derivation and explanations of this framework in the literature[51]. For the sake of simplicity and lightness, it is sufficient for us to understand how to extract the conductivity from the Boltzmann equation. The energy dispersion evolves with the electric field:

$$\frac{d\varepsilon(t)}{dt} = \frac{d\mathbf{k}}{dt} \cdot \mathbf{v}(\mathbf{k}(t)) = -e\mathbf{E} \cdot \mathbf{v}(\mathbf{k}(t)) \implies \varepsilon(t) = \varepsilon(0) - e\mathbf{E} \cdot \int_0^t \mathbf{v}(\mathbf{k}(t')) dt' \quad (5)$$

By definition, the steady-state current (but still in presence of perturbation) depends on the out-of-equilibrium distribution function and the velocities, while the elements of the conductivity tensor define the relation between the components of the current and the applied field:

$$\begin{aligned} \mathbf{J} &= -e \int_{\mathbf{k}} \mathbf{v}(\mathbf{k}) f(\mathbf{k}) \\ \sigma_{ij} \equiv \frac{\partial J_i}{\partial E_j} &= -e \int_{\mathbf{k}} v_i \frac{\partial f(\mathbf{k})}{\partial E_j} \end{aligned}$$

---

<sup>6</sup>The “width” of the FS because of thermal fluctuations only becomes relevant at the Fermi temperature  $T_F \sim 10^4 K$ . The main temperature-dependence of resistivity will be given by the scattering rate, and hence we will consider only states on the FS as if  $T = 0$ .

Combining eqs.5 and 4, one arrives at the steady state distribution, in which time only appears parametrizing the orbit in k-space:

$$f(\mathbf{k}) = f_0(\mathbf{k}) - e\mathbf{E} \cdot \int_{-\infty}^0 dt \left( \frac{df_0}{d\varepsilon} \Big|_{\varepsilon(t)} \right) \mathbf{v}(\mathbf{k}) \exp \left( - \int_0^t dt' / \tau(\mathbf{k}(t')) \right)$$

Finally, one can directly input this last equation in the current definition and read the expresion for the conductivity, which is called **Chamber's formula**. This will be our main theoretical tool to extract information from our experiments. At low temperatures, one considers only states on the Fermi surface, and introduces the density of states (DoS), wich is the inverse of the velocity modulus, resulting in a final expression:

$$\rho_{ij}^{-1} \equiv \sigma_{ij} = e^2 \int_{FS} \frac{d\mathbf{k}}{(2\pi)^3} \int_0^\infty dt \frac{\nu_i(\mathbf{k}) \nu_j(\mathbf{k}(t))}{\hbar |\mathbf{v}(\mathbf{k})|} \exp \left( - \int_0^t \frac{dt'}{\tau(\mathbf{k}(t'))} \right) \quad (6)$$

Let us try to develop some physical intuition from this equation. One might naively think that the magnetic field has dissappeared, but it is precisely the quantity which defines the orbits  $\mathbf{k}(t)$ , through eq.1. Then, one is integrating the velocity along these orbits, convoluted with a term that damps such orbit over a timescale given by the scattering rate. This term is a sort of average of the velocity along the orbit taking into account the probability of scattering out of it at every point. Then, this average is further convoluted with the velocity in the direction "of interest" in which we are measuring current. In plane words, one is comparing "how much" of the initial velocity is still in this direction after averaging over the orbits caused by the magnetic field<sup>7</sup>. Based on this result then, we can obtain the resistivity tensor  $\rho = \sigma^{-1}$  that we will measure during the experiment, if we know the dispersion relation in the Fermi surface and the shape of the scattering rate.

It is here where one can access the information from the experiment. Our approach is based on proposing a correct Tight Binding (TB) model  $\varepsilon(\mathbf{k})$  to determine  $\mathbf{v}(\mathbf{k})$ , and suitable considerations for the scattering rate  $\tau(\mathbf{k})$ , running a simulation of this equation and fitting the results to the ADMR measurements.

## 4 Measurement: ADMR in extreme magnetic fields

As we have seen, complete orbits around the Fermi surface give rise to observable oscillations in the resistivity, because of the averaging of velocities. These oscillations contain important information on the Fermi surface and the scattering of electrons within the material. The frequency with which this orbits can be completed depends on some material parameters such as the effective mass, but also in the external magnetic field:

$$\omega_c = \frac{qB}{m^*}$$

Since the scattering rate is fixed, the only way we have to enhance these oscillations is by using extreme magnetic fields. This is specially important when one expects a scattering

---

<sup>7</sup>If looked at carefully, this equation resembles the quantum current-current correlation function that defines the conductivity in linear response theory, but as a classical version. We expect it to be true then in the regime where the quasiparticle picture holds and the electrons can be described as wavepackets of wavelength much smaller than their mean free path.

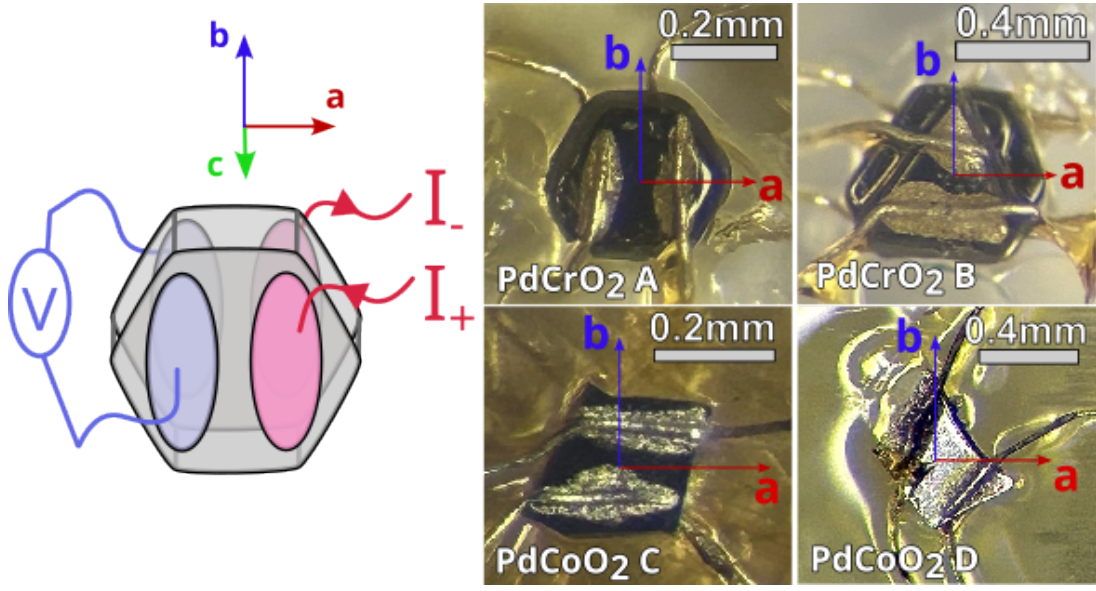


Figure 6: **Our set of samples and the contact configuration.** (Left) Our 4-point contact configuration for the measurements. The width of the sample is of the order of  $\sim 10\mu\text{m}$ , much less than the electronic mean free path. For this reason the measurements will still give reliable results. (Right) Our 4 samples at scale. Samples A & B are  $\text{PdCrO}_2$  while samples C & D are  $\text{PdCoO}_2$ . The indicated axis are the lattice vectors of the conventional cell, with the missing vector  $\vec{c}$  pointing upwards towards the reader.

rate of the order of the Planckian limit. For this reason, we performed our experiments in the largest resistive continuous magnet that exists at the moment, the Cell 6 magnet at the National High Magnetic Fields Laboratory (NHMFL) in Tallahassee, Florida, which can achieve up to 42T in continuous field. During the span of 5 days, we recollected data in 4 samples, 2  $\text{PdCrO}_2$  and 2  $\text{PdCoO}_2$ , covering the temperature range from 15 to 100K (in 13 total steps) systematically, while rotating the polar  $\theta$  and azimuthal  $\phi$  angles.

#### 4.1 Preparation of the samples

Our delafossites were grown by the group of professor Alannah Hallas, at University of British Columbia, using the liquid flux growth method[42, 52]. Our objective is to measure the voltage drop across the oxide layers, which we will call c-axis resistivity or  $\rho_{zz}$  (current and voltage measured along the z direction).

These samples are extremely small, less than 1mm in most cases, and even hard to see by the naked eye. This is the main reason for the difficulty of the transport experiment preparation, of which the main part is putting contacts to allow for a 4-point measurements. This task was performed by Adrien Gourgout at the Laboratoire des Solides Irradiés. The contacts were made with silver epoxy Dupont 6838. For oxide materials like the ones we are treating, a thin oxide layer always exist on the surface if the sample is handled in atmospheric conditions. Such layer is insulating, therefore, to ensure a good electrical continuity, the sample is heated up to 400°C, allowing the silver epoxy to diffuse through the oxide layer and into the material. Moreover, due to the unusual shape that these crystals acquire when they are grown, the location of the contacts is not typical of simple quasi2D materials like cuprates. It is worth to take a look and justify such measurement geometry.

A scheme of the configuration can be seen and the real samples can be seen in Fig.6.

To perform c-axis experiments, one would like to have well defined shape for the sample, with an aspect ratio allowing for an easy 4-point configuration. However, our materials are quasi-2D, and therefore the contacts imposing the current and the ones measuring voltage must lie in the same plane. At first glance, this configuration is undesired, since voltage would be measured in a different spatial region than where current is passing. In our case, the strong in-plane/out-of-plane anisotropy of transport,  $\rho_{zz}/\rho_{xx} \sim 1000$ [37] and the small size of our samples justifies such configuration. In other words, electrons diffuse very fast along the plane before inter-plane transport occurs. This means that current will diffuse rapidly from the current-giving contact to the voltage gauge and the difference in density current between these different places will be negligible. This configuration has been previously used to measure these materials successfully[46].

## 4.2 Performing the experiment under extreme magnetic fields

Once the samples are prepared, they need to be placed in the rotating probe with some thought. The rotating probe can allocate a cylindrical sample holder of  $\sim 2$  cm. The caps of the cylinder were used to hold the samples and the electrical terminals connecting them to the exterior control of the experiment. The 4 samples were measured simultaneously and under the same conditions of field and temperature, to make the comparison of the data as reliable as possible. To ensure that the samples did not move during rotation, one flat side of the sapphire substrate was aligned with the lattice vector  $\vec{a}$  of the delafossites' unit cell, and then stuck to the plane of the sample holder. In this configuration, the c-axis of the samples starts perpendicular to the field direction. Given the rotation motor of the probe, our range of rotation in  $\theta$  is from  $50^\circ$  to  $280^\circ$ , although the full range could not be used due to lack of time. The sample holder is rotated by a mechanical rotator located at the top of the magnet which pulls two strings that are wound around the mount[53] (see Fig.7). We digitally convert the rotation units to the angle that has been rotated. The azimuthal  $\phi$  angle is easily changed simply by rotating the cylinder around its own axis (see scheme in Fig.7). To align such an angle to the desired one, we took pictures with respect to the original configuration and used digital tools to calculate the reference point accurately, finally performing such alignment visually.

The magnets at NHMFL are incredible engineering achievements. Our specific magnet was the Cell 6 resistive magnet, capable of achieving a continuous field of 42T, the highest in the world. The magnet, of three meter of height and around two of diameter, consumes 32 megawatts at maximum field<sup>8</sup>. At this power, the copper coils that produce the field would sublime in a few seconds due to Joule effect. To avoid this, the NHMFL uses a cooling system with capacity of 15.000 litter of water per minute, using support from a nearby lake. In total, and at current local electricity price, our experiment costed the magnet lab around 100.000\$. The samples are inserted into a chamber of 32 mm in which the field is homogeneous. To do this, the cell also has a variable temperature inset (VTI) which can cover the range from 0.3K to 300K. To control the temperature, we used PDI's from LakeShore 330. The current was fixed using SRS current sources, whose signal was produced by our SRS 860 lock-ins. The same lock-ins were used to measure the voltage resulting in our final resistivity curves.

---

<sup>8</sup>The carbon footprint and the water expenses of experiments like these is not negligible at all. I believe it is important to take this into account if one wants to continue in this line of research. There are more high-magnetic-field facilities in Europe, however they did not have the rotating mount that we needed for ADMR. This is also a reason to develop our own in-home rotator, so we can adapt to any facility we visit.

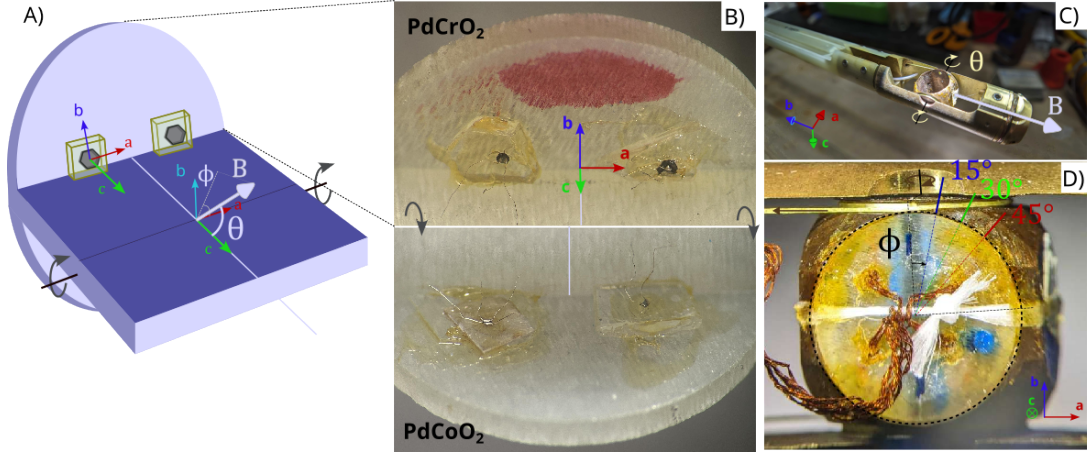


**Figure 7: Sample holder and the rotator.** (A) Schematics of the sample holder. The magnetic field orientation is indicated in the crystalline basis. Our initial position is  $\mathbf{B} \perp \vec{c}$ . The polar angle  $\theta$  is explored by rotating the axis perpendicular to the sample holder walls (black arrows), while the azimuthal angle  $\phi$  is explored rotating around the  $\vec{c}$  axis. Only two samples are indicated, the other two would be on the same location, but below the plane. In the opposite walls, there are the wires connecting the samples to the measurement equipment. (B) Picture of our 4 samples. The samples are shown in the same order as in Fig.6. A flat section of the Silica substrate is oriented with the  $\vec{a}$  lattice vector and with the plane of the sample holder, to ensure that the samples do not move when rotating. (C) Rotating mount. This hollow cylinder is connected to a mechanical rotator through the small chords that wind around its lateral caps. It is located at the tip of a 4-meter tall VTI that is inserted in the magnet. (D) Close up of the rotator. The chords used to rotate the sample are more visible in this picture (brown arrows). The azimuthal angles explored in the experiment are indicated.

## 5 Results

In this section, I present the results obtained during our measurements in the NHMFL and our initial qualitative analysis. During our productive week, we obtained around 300 curves that were properly scaled and offseted, to perform a posterior fit using our described models.

### 5.1 Results of the measurements at the NHMFL

For the sake of clarity and consistency, I only present some results of our measurements for our cleanest samples. The comparison between both materials is easier to do in these cases because of the quality of the curves. However, many other interesting observations can be done for the rest of our samples which show reproducibility and will help us to perform a more precise simulation. The interested reader can find a summary of these observations in the Annex A

Let us start by the general observations. The ADMR curves show very clean oscillations due to the high magnetic field, and we immediately observe a very clear dependence with the azimuthal angle (see Fig.8). This will allow us to better fine-tune the dispersion along the  $k_z$  direction. Another important concept we observe is that the curves are perfectly symmetric across  $\theta = 180^\circ$ , which we knew had to be the case because of the configuration of our samples (see scheme in Fig.7).

The main reason to measure both materials at the same time and under the same conditions is to be able to have reliable comparisons. In Fig.8, I select measurements in the

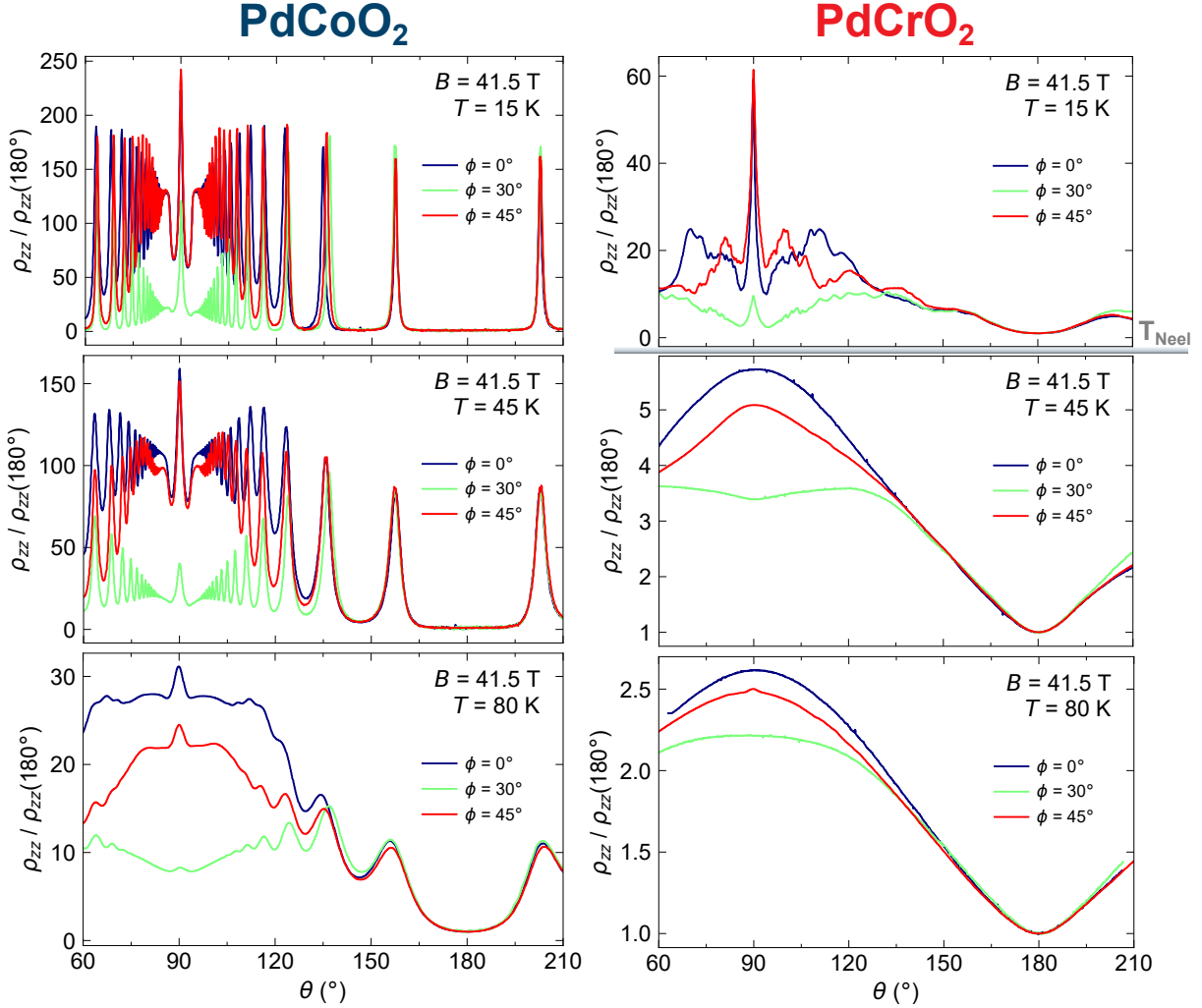


**Figure 8: Main results of the measurements.** At 15K, our data show the most striking difference. In PdCoO<sub>2</sub>, there is no AFM phase. Its Fermi surface remains unchanged, and we observe regular and fast oscillations all the way up to 100K. For PdCrO<sub>2</sub>, in the AFM phase, ADM reveals a rich display of smaller oscillations, following the folding of the Brillouin Zone caused by the new periodicity imposed by the AFM order. This is the reason why we observe such contrast in our data at 15K, despite both materials behaving like good metals. Above the Néel Temperature at 37.5K, both materials have the same Fermi surface. However, the oscillations in the ADMR of PdCrO<sub>2</sub> are completely damped by the sudden rise in the scattering rate that seems to occur right above of the AFM transition. Despite the prominent features being smoothed out, we are still left with some important similarities in the  $\phi$  angle, this is particularly visible when one compares PdCoO<sub>2</sub> at T = 80K and PdCrO<sub>2</sub> at T = 45 K. Indeed, once can see that the  $\phi$  dependence is the same at  $\theta = 90^\circ$ , with a dip for  $\phi = 30^\circ$ , and a maximum for  $\phi = 0^\circ$ .

low, middle and high temperature regimes and compare the results of the samples PdCrO<sub>2</sub> A and PdCoO<sub>2</sub> D (our cleanest samples). Below the Néel temperature, the results are very different. PdCoO<sub>2</sub> shows the expected result for a regular quasi-2D material with corrugations along  $k_z$ , a series of peaks at the so-called Yamaji angles[54], related to orientations of the field in which the velocity along the z direction is very well averaged<sup>9</sup>. These peaks are present in the entirety of our range of temperatures, and they seem not to change loca-

<sup>9</sup>To understand this, consider that, for certain orbits, the component  $v_z$  has opposite sign in opposite points of the orbit at all times, and hence  $v_z$  is very well averaged.

tion. This means that the FS is unchanged, and since the only reason for the oscillations to be smeared is the scattering rate, we can in principle say that  $1/\tau$  increases slowly with temperature. This is not at all the case for PdCrO<sub>2</sub>. In the AFM phase, ADMR shows a large amount of small features like peaks and shoulders that do not resemble the data of PdCoO<sub>2</sub>. This is expected if the FS of the material undergoes magnetic reconstruction in this phase. However, as explained before, it is not clear that at these large fields the AFM survives and with it the folded FS. The simulations will help us understand better this concept, which may be in itself a different project. Immediately above the AFM transition, we start seeing consistency with our expectations. PdCrO<sub>2</sub> loses all of its features, which are now completely smeared. These results are what is expected in the regime where  $\omega_c \tau \lesssim 1$ , meaning that the scattering rate dominates and the orbits are not completed. Using results from quantum oscillations[35], the mass along the orbits in PdCrO<sub>2</sub> is  $m^* \sim 1.5m_e$ , with  $m_e$  the electron mass. Therefore  $\omega_c = e/m^*B \sim 5 \cdot 10^{12} s^{-1}$  at 42 Tesla, while, at 45K, the Planckian scattering rate gives  $\tau = \hbar/k_B T \sim 1.7 \cdot 10^{-13} s$ , resulting in  $\omega_c \tau \sim 1$ . Hence, ADMR is showing consistent results with PdCrO<sub>2</sub> achieving the Planckian rate above its Néel temperature. This is in agreement with what we expected from the AFM fluctuations in this regime, a scattering rate that quickly rises towards the Planckian bound. These are far from definite results, an explicit T-linear dependence is needed to convince ourselves. However, they represent qualitative observations of what we expected.

Finally, one can recognize the similarities between the curves for PdCoO<sub>2</sub> at 80K and those of PdCrO<sub>2</sub> at 45K for the same azimuthal angles. If we were to measure at lower fields or higher temperatures, the curves of PdCoO<sub>2</sub> would be very similar to those of PdCrO<sub>2</sub>. This is solely related to the fact that both Fermi surfaces are very similar at high T.

## 5.2 Preliminary simulations for PdCoO<sub>2</sub>

As I mentioned, the analysis of the ADMR data necessitates of numerical simulations of the experiment. Their objective will be therefore to fit the Fermi surface for both materials, for which we expect similar results, and extract the scattering rate dependence with  $\mathbf{k}$  and T at the same time. Our simulations run essentially in 3 steps. First, the Fermi surface is calculated from a Tight Binding (TB) model. Then, the Boltzmann orbits along such surface are calculated from eq.1 and the integral over time of eq.6 is performed. Afterwards, we numerically evaluate the remaining integral to obtain the conductivity. Finally, the polar angle of the magnetic field is changed and we repeat the procedure until the complete curve is reproduced. This represents one measurement at fixed temperature and azimuthal angle  $\phi$ , and takes approximately 10 seconds. One can see how the fitting quickly becomes very energy and time-consuming. Once we obtained the data, my main occupation was to adapt this code to the case of our delafossites, which is not a straightforward task as I explain in this section.

If we want to perform absolute-value simulations of transport, it is imperative that we achieve to correctly describe the Fermi Surface quantitatively. This necessarily implies that we need to take into account the possibly complicated Brillouin Zone boundaries of the material. So far, the group had centered its studies in materials with tetragonal lattice structure, mainly cuprates. The in-house code for the obtention of the Fermi Surface at the time I joined was based on discretizing the Brillouin Zone (BZ) with a simple rectangular meshgrid. This code have proved really successful in reproducing the ADMR data, see for example Fig.5 whose simulation was done using our code. For this straightforward structure, not many

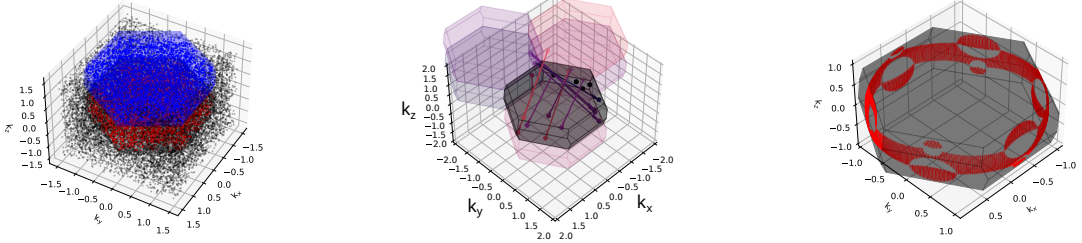


**Figure 9: The results of my calculations for the delafossites' Brillouin Zone.** The code identifies in which Brillouin Zone the points are (**left**), and maps it back to the first one (**center**). The algorithm can generate 3D Fermi surfaces in complex Brillouin Zone geometries like the one of delafossites (**right**). The Fermi surface shown corresponds to an arbitrary isotropic dispersion  $\varepsilon \sim |\vec{k}|^2$ . Notice how the portions of the sphere gets reflected back inside the 1st BZ despite the complex boundary symmetries.

special considerations are needed, one can just fixate in the first BZ for the analysis. However, if the shape of the Brillouin Zone is more complicated, it will impose different periodic boundary conditions to the Fermi Surface.

One of my main contributions during the internship apart from the measurements was to generalize the construction of Fermi Surfaces to arbitrary Brillouin Zones. This was necessary for the study of  $\text{PdCoO}_2$ , since its structure is not as simple as the case of cuprates or nickelates. For this, I based myself in the pymatgen package, a well developed tool to study lattice structure and symmetries in python. In the present text, I will only present the idea and results, but the interested reader can find a complete report of this development here.

The pymatgen package allows the user to obtain the structure of a material if it exists in the *Materials Project* website, an official database for material physics and chemistry that contains very complete information for thousands of materials. From this website, the user can obtain a file, with format .cif, containing the complete information of the material. The code I develop can use this file to read and generate the first Brillouin Zone. Afterwards, it creates a rectangular grid using the limits of such zone, checks which points belong to the first BZ, and stores them. The program can now generate the Fermi Surface from these points. However, it is still possible that some points of the Fermi Surface lie in the neighbouring BZ's, and should therefore be translated back using the lattice vectors. This is another important part of the code, which generates collinear Brillouin Zones, checks which points are in there, and translates the corresponding Fermi Surfaces back to the first Brillouin Zone. I present some results in Fig.9, in which I show how the code is able to detect which points are in which Brillouin Zone, and also translate those back to the first one. Finally, this can be used to create complex Fermi Surfaces in arbitrary Brillouin Zones using the `scipy marching_cubes` algorithm.

During my internship I also made other contributions related to numerical simulations, for example a code to generate band diagrams from non-diagonal dispersions and high-symmetry points on k-space from the same .cif file generating the 1st Brillouin Zone. We used this code to diagonalize the s-p hybrid bands of the infinite-layer Lanthanum nickelates[55]. Apart from generating the correct band diagram and the Fermi surface, our code is able to reproduce the absolute value for the Seebeck effect observed in  $\text{NdNiO}_2$  measurements[56] (see AnnexB).

As seen, a correct dispersion is fundamental for the simulation. For our tight binding

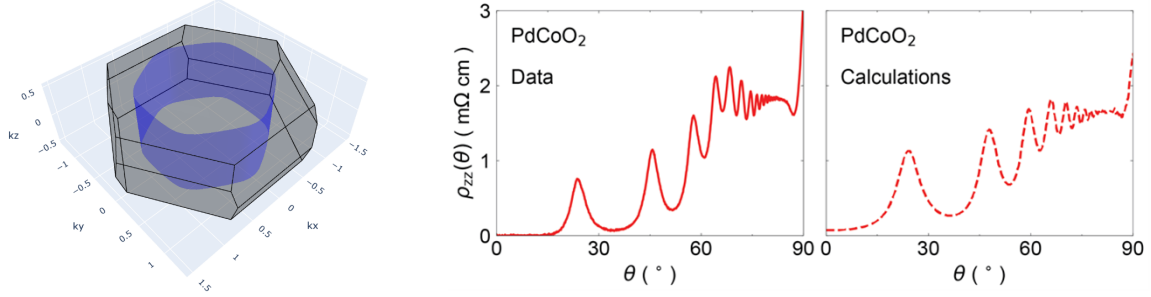


Figure 10: **Current state of the simulations for  $\text{PdCoO}_2$ .** (Left) Simulation of the  $\text{PdCoO}_2$  Fermi surface in the correct Brillouin Zone. (Right) Preliminary simulations compared with ADMR observations in  $\text{PdCoO}_2$ .

model, we base ourselves in DFT+DMFT calculations and ARPES measurements. In the case of the delafossites however, there are some caveats that are worth mentioning. ARPES and DFT can only generate 2D Fermi surfaces, on the  $k_x$  and  $k_y$  plane. This necessarily means that we can only obtain the in-plane hopping terms from these measurements. Due to the 2D considerations, even the high symmetry points  $K$  and  $M$  are not the ones from the real Brillouin Zone (see Fig.9). Therefore, the out-of-plane hopping, which is fundamental to reproduce ADMR measurements, cannot be simply fitted to the band in this case.

To overcome this obstacle, we base ourselves in the fact that the ratio between in-plane and out-of-plane hopping terms follow the ratio of the in-plane and out-of-plane resistivity,  $\rho_{zz}/\rho_{xx} \sim 1000$ . Hence, once we have the correct Brillouin Zone, it would be necessary to calculate a set of transport coefficients like the Hall coefficient or the zero temperature resistivity for different  $t_z/t$  values and fit to the observed behaviour in literature[37]. This will likely be the work of my last month of internship. While I cannot provide precise values for our TB parameters, I can motivate our approach by showing that the simulations can already qualitatively describe the ADMR curves both in shape and absolute value (see Fig.10) for a lazily-fitted value of  $t/t_z \sim 1000$ .

As a summary, the required simulations are very consuming in terms of power and time, and cannot be done by an ordinary computer. We must have at least some certainty that the code is giving correct results for already-known results if we want to have hope of describing correctly our observations. This passes through a correct BZ description, TB model and scattering rate considerations. As a precedent, previous work of my supervisor which followed a similar approach took around 2 years between obtention of the measurements, analysis and publication[45]. This is the current state of the project, which will be continued during my PhD.

## 6 Conclusion

I believe that doing an internship should not only mean to learn about what it is done in the laboratory. The life of a researcher is composed of many more experiences one needs to be comfortable with, both nice ones like seeing new places and meeting new colleagues, or not-so-nice ones like sleeping very little to ensure your experiment works or living a full week on caffeine. Being aware of how rare is that a M2 intern gets to experience all of this, I must say I feel extremely lucky to participate in a wide range of experiences that have assured my motivation for the future. Since I believe they were also important parts of my internship,

I believe it is worth to dedicate a few words to them. To begin with, I had the luck to participate in big-facility experiments in a different country, which allowed me not only to get the experience of achieving high quality data but also to collaborate with numerous individuals, and learn from their personal careers and crafts. I was also invited to participate in a conference, the International Research Laboratory (IRL) annual symposium in Jouvence, Quebec, my first ever, in which I also presented our work in the form of a poster. I also was lucky enough to participate in the GDR MEETICC school on Topology, in which I enhanced my knowledge on topology and connected with many PhD students from several parts of France, which I am sure I will meet again in my next stage at the Laboratoire des Solides Irradiés. I also presented my poster in this occasion, and I was excited to see the discussion that our work sparked and the amount of interesting question that are still to be answered.

In terms of our work, much remains to be done. A complete generalization of our simulation code will allow us to explore much more materials and perform much faster analysis. In the long run, we have ideas of developing a more involved software which would not necessarily include the relaxation time approximation, but would work in the general scattering matrix formalism. This would allow us to explore much more complicated behaviour and could open the door to very complex transport simulations. As for our data, the next step is to perform the fit that will allow us to extract the temperature dependence of the scattering rate, as well as the  $\mathbf{k}$ -dependence. This is referring to the high temperature regime, while for the low temperature regime we can investigate other concepts with our data like the magnetic reconstruction of  $\text{PdCrO}_2$  under its Néel temperature. Once the fit is done, we can also move our focus towards other interesting experimentally-accessible properties of these materials like the Seebeck coefficient or the in-plane transport, which should give us further information on how the antiferromagnetic fluctuations of  $\text{PdCrO}_2$  are affecting the electronic transport. Finally, since the group is still starting to walk, much work will be dedicated to the setup of a completely new transport laboratory in École Polytechnique, which will give me the opportunity to learn every single aspect of the job of a multifaceted experimental physicist.



**Figure 11: Experiences during my internship.** **(Top-Left)** Picture with the PhD students of the GDR MEETICC Topology summer school in the French Alps, Aussois, France. **(Top-Right)** Picture at the Cell 6, NHMFL. From right to left: David Graf, Gaël Grissonnanche, and myself. **(Bottom)** Picture at the IRL Colloque in Jouvence, Canada.

## References

- [1] R. Daou et al. “Linear Temperature Dependence of Resistivity and Change in the Fermi Surface at the Pseudogap Critical Point of a High-T<sub>c</sub> Superconductor”. In: *Nature Physics* 5.1 (Jan. 2009), pp. 31–34. ISSN: 1745-2473, 1745-2481. DOI: 10.1038/nphys1109. (Visited on 06/18/2024).

- [2] P. Fournier et al. “Insulator-Metal Crossover near Optimal Doping in  $\{\{Pr\}_{2-x}\}Ce_x\{CuO\}_4$ : Anomalous Normal-State Low Temperature Resistivity”. In: *Physical Review Letters* 81.21 (Nov. 1998), pp. 4720–4723. DOI: 10.1103/PhysRevLett.81.4720.
- [3] S. Martin et al. “Normal-State Transport Properties of  $\{\mathrm{Bi}\}_{2+x}\{\mathrm{Sr}\}_{y}\{\mathrm{CuO}\}_{6+\delta}$  Crystals”. In: *Physical Review B* 41.1 (Jan. 1990), pp. 846–849. DOI: 10.1103/PhysRevB.41.846.
- [4] Nicolas Doiron-Leyraud et al. “Correlation between Linear Resistivity and  $T_c$  in the Bechgaard Salts and the Pnictide Superconductor  $Ba(Fe_{1-x}Co_x)_2As_2$ ”. In: *Physical Review B* 80.21 (Dec. 2009), p. 214531. ISSN: 1098-0121, 1550-235X. DOI: 10.1103/PhysRevB.80.214531. (Visited on 06/14/2024).
- [5] H. v. Löhneysen et al. “Non-Fermi-liquid Behavior in a Heavy-Fermion Alloy at a Magnetic Instability”. In: *Physical Review Letters* 72.20 (May 1994), pp. 3262–3265. DOI: 10.1103/PhysRevLett.72.3262.
- [6] Philip W Phillips, Nigel E Hussey, and Peter Abbamonte. “Stranger than metals”. In: *Science* 377.6602 (2022), eabh4273.
- [7] B. Michon et al. “Thermodynamic Signatures of Quantum Criticality in Cuprate Superconductors”. In: *Nature* 567.7747 (Mar. 2019), pp. 218–222. ISSN: 1476-4687. DOI: 10.1038/s41586-019-0932-x.
- [8] P. Walmsley et al. “Quasiparticle Mass Enhancement Close to the Quantum Critical Point in  $\{BaFe\}_2\{As\}_{1-x}\{P\}_x\}_2$ ”. In: *Physical Review Letters* 110.25 (June 2013), p. 257002. DOI: 10.1103/PhysRevLett.110.257002.
- [9] S. Nakamae et al. “Electronic Ground State of Heavily Overdoped Nonsuperconducting  $\{\mathrm{La}\}_{2-x}\{\mathrm{Sr}\}_x\{\mathrm{CuO}\}_4$ ”. In: *Physical Review B* 68.10 (Sept. 2003), p. 100502. DOI: 10.1103/PhysRevB.68.100502.
- [10] Bom Soo Kim, Elias Kiritsis, and Christos Panagopoulos. “Holographic Quantum Criticality and Strange Metal Transport”. In: *New Journal of Physics* 14.4 (Apr. 2012), p. 043045. ISSN: 1367-2630. DOI: 10.1088/1367-2630/14/4/043045.
- [11] Subir Sachdev. “Condensed Matter and AdS/CFT”. In: vol. 828. 2011, pp. 273–311. DOI: 10.1007/978-3-642-04864-7\_9. arXiv: 1002.2947 [cond-mat, physics:hep-th].
- [12] Sean A. Hartnoll and Andrew P. Mackenzie. “Colloquium : Planckian Dissipation in Metals”. In: *Reviews of Modern Physics* 94.4 (Nov. 2022), p. 041002. ISSN: 0034-6861, 1539-0756. DOI: 10.1103/RevModPhys.94.041002. (Visited on 05/24/2024).
- [13] A. Legros et al. “Universal T-linear Resistivity and Planckian Dissipation in Overdoped Cuprates”. In: *Nature Physics* 15.2 (Feb. 2019), pp. 142–147. ISSN: 1745-2481. DOI: 10.1038/s41567-018-0334-2.
- [14] Alexandre Jaoui et al. “Quantum Critical Behaviour in Magic-Angle Twisted Bilayer Graphene”. In: *Nature Physics* 18.6 (June 2022), pp. 633–638. ISSN: 1745-2481. DOI: 10.1038/s41567-022-01556-5.
- [15] Yoichi Ando et al. “Electronic Phase Diagram of High- $T_c$  Cuprate Superconductors from a Mapping of the In-Plane Resistivity Curvature”. In: *Physical Review Letters* 93.26 (Dec. 2004), p. 267001. ISSN: 0031-9007, 1079-7114. DOI: 10.1103/PhysRevLett.93.267001. arXiv: cond-mat/0403032. (Visited on 06/18/2024).

- [16] A. W. Tyler et al. “High-Field Study of Normal-State Magnetotransport in  $Tl_2Ba_2CuO_{6+\delta}$ ”. In: *Physical Review B* 57.2 (Jan. 1998), R728–R731. ISSN: 0163-1829, 1095-3795. DOI: 10.1103/PhysRevB.57.R728. (Visited on 06/18/2024).
- [17] Tao Hu et al. “Universal Linear-Temperature Resistivity: Possible Quantum Diffusion Transport in Strongly Correlated Superconductors”. In: *Scientific Reports* 7.1 (Aug. 2017), p. 9469. ISSN: 2045-2322. DOI: 10.1038/s41598-017-09792-z.
- [18] Subir Sachdev. “Quantum Phase Transitions”. In: () .
- [19] J. A. N. Bruin et al. “Similarity of Scattering Rates in Metals Showing  $T$ -Linear Resistivity”. In: *Science* 339.6121 (Feb. 2013), pp. 804–807. ISSN: 0036-8075, 1095-9203. DOI: 10.1126/science.1227612.
- [20] J. Chang et al. “Anisotropic Breakdown of Fermi Liquid Quasiparticle Excitations in Overdoped  $La_2-xSrxCuO_4$ ”. In: *Nature Communications* 4.1 (Oct. 2013), p. 2559. ISSN: 2041-1723. DOI: 10.1038/ncomms3559.
- [21] Bastien Michon et al. “Reconciling Scaling of the Optical Conductivity of Cuprate Superconductors with Planckian Resistivity and Specific Heat”. In: *Nature Communications* 14.1 (May 2023), p. 3033. ISSN: 2041-1723. DOI: 10.1038/s41467-023-38762-5.
- [22] Sudip Chakravarty, Bertrand I. Halperin, and David R. Nelson. “Low-Temperature Behavior of Two-Dimensional Quantum Antiferromagnets”. In: *Physical Review Letters* 60.11 (Mar. 1988), pp. 1057–1060. ISSN: 0031-9007. DOI: 10.1103/PhysRevLett.60.1057.
- [23] Sudip Chakravarty, Bertrand I. Halperin, and David R. Nelson. “Two-Dimensional Quantum Heisenberg Antiferromagnet at Low Temperatures”. In: *Physical Review B* 39.4 (Feb. 1989), pp. 2344–2371. ISSN: 0163-1829. DOI: 10.1103/PhysRevB.39.2344.
- [24] N. Doiron-Leyraud et al. “Linear-T Scattering and Pairing from Antiferromagnetic Fluctuations in the  $(TMTSF)_{2X}$  Organic Superconductors”. In: *The European Physical Journal B* 78.1 (Nov. 2010), pp. 23–36. ISSN: 1434-6036. DOI: 10.1140/epjb/e2010-10571-4.
- [25] Cyril Proust and Louis Taillefer. “The Remarkable Underlying Ground States of Cuprate Superconductors”. In: *Annual Review of Condensed Matter Physics* 10.1 (Mar. 2019), pp. 409–429. ISSN: 1947-5454, 1947-5462. DOI: 10.1146/annurev-conmatphys-031218-013210.
- [26] J. Zaanen. “Superconductivity - Why the Temperature Is High”. In: *Nature* 430 (Aug. 2004), pp. 512–3. DOI: 10.1038/430512a.
- [27] Yanan Zhang et al. *High-Temperature Superconductivity with Zero-Resistance and Strange Metal Behavior*. Apr. 2024. arXiv: 2307.14819 [cond-mat].
- [28] Yuan Cao et al. “Strange Metal in Magic-Angle Graphene with near Planckian Dissipation”. In: *Physical Review Letters* 124.7 (Feb. 2020), p. 076801. ISSN: 0031-9007, 1079-7114. DOI: 10.1103/PhysRevLett.124.076801. (Visited on 06/18/2024).
- [29] G. R. Stewart. “Unconventional Superconductivity”. In: *Advances in Physics* 66.2 (Apr. 2017), pp. 75–196. ISSN: 0001-8732. DOI: 10.1080/00018732.2017.1331615.
- [30] Pengcheng Dai et al. “Resonance as a Measure of Pairing Correlations in the High-Tc Superconductor  $YBa_2Cu_3O_{6.6}$ ”. In: *Nature* 406.6799 (Aug. 2000), pp. 965–968. ISSN: 0028-0836, 1476-4687. DOI: 10.1038/35023094. (Visited on 06/18/2024).

- [31] F. Essunger et al. "Superconducting Pairing Mediated by Spin Fluctuations from First Principles". In: *Physical Review B* 90.21 (Dec. 2014), p. 214504. ISSN: 1098-0121, 1550-235X. DOI: 10.1103/PhysRevB.90.214504.
- [32] D. J. Scalapino. "A Common Thread: The Pairing Interaction for Unconventional Superconductors". In: *Reviews of Modern Physics* 84.4 (Oct. 2012), pp. 1383–1417. ISSN: 0034-6861, 1539-0756. DOI: 10.1103/RevModPhys.84.1383.
- [33] J. R. Schrieffer, X. G. Wen, and S. C. Zhang. "Dynamic Spin Fluctuations and the Bag Mechanism of High- $T_c$  Superconductivity". In: *Physical Review B* 39.16 (June 1989), pp. 11663–11679. DOI: 10.1103/PhysRevB.39.11663.
- [34] A P Mackenzie. "The Properties of Ultrapure Delafossite Metals". In: *Reports on Progress in Physics* 80.3 (Mar. 2017), p. 032501. ISSN: 0034-4885, 1361-6633. DOI: 10.1088/1361-6633/aa50e5.
- [35] Clifford W. Hicks et al. "Quantum Oscillations and Magnetic Reconstruction in the Delafossite PdCrO<sub>2</sub>". In: *Physical Review B* 92.1 (July 2015), p. 014425. ISSN: 1098-0121, 1550-235X. DOI: 10.1103/PhysRevB.92.014425.
- [36] Elina Zhakina et al. "Investigation of Planckian Behavior in a High-Conductivity Oxide: PdCrO<sub>2</sub>". In: *Proceedings of the National Academy of Sciences* 120.36 (Sept. 2023), e2307334120. ISSN: 0027-8424, 1091-6490. DOI: 10.1073/pnas.2307334120.
- [37] Clifford W. Hicks et al. "Quantum Oscillations and High Carrier Mobility in the Delafossite PdCoO<sub>2</sub>". In: *Physical Review Letters* 109.11 (Sept. 2012), p. 116401. ISSN: 0031-9007, 1079-7114. DOI: 10.1103/PhysRevLett.109.116401.
- [38] Xiaoping Yao et al. "Origin of the High Electrical Conductivity of the Delafossite Metal PdCoO<sub>2</sub>". In: *Physical Review B* 109.7 (Feb. 2024), p. 075110. ISSN: 2469-9950, 2469-9969. DOI: 10.1103/PhysRevB.109.075110.
- [39] Han-Jin Noh et al. "Anisotropic Electric Conductivity of Delafossite PdCoO<sub>2</sub> Studied by Angle-Resolved Photoemission Spectroscopy". In: *Physical Review Letters* 102.25 (June 2009), p. 256404. ISSN: 0031-9007, 1079-7114. DOI: 10.1103/PhysRevLett.102.256404.
- [40] Jonathan A. Sobota et al. "Electronic Structure of the Metallic Antiferromagnet Pd-CrO<sub>2</sub> Measured by Angle-Resolved Photoemission Spectroscopy". In: *Physical Review B* 88.12 (Sept. 2013), p. 125109. ISSN: 1098-0121, 1550-235X. DOI: 10.1103/PhysRevB.88.125109. arXiv: 1309.1374 [cond-mat].
- [41] Frank Lechermann. "From Basic Properties to the Mott Design of Correlated Delafossites". In: *npj Computational Materials* 7.1 (July 2021), p. 120. ISSN: 2057-3960. DOI: 10.1038/s41524-021-00586-6.
- [42] Yi Zhang et al. "Crystal-Chemical Origins of the Ultrahigh Conductivity of Metallic Delafossites". In: *Nature Communications* 15.1 (Feb. 2024), p. 1399. ISSN: 2041-1723. DOI: 10.1038/s41467-024-45239-6.
- [43] Nabhanila Nandi et al. "Unconventional Magneto-Transport in Ultrapure PdCoO<sub>2</sub> and PtCoO<sub>2</sub>". In: *npj Quantum Materials* 3.1 (Dec. 2018), p. 66. ISSN: 2397-4648.
- [44] R. A. Matula. "Electrical Resistivity of Copper, Gold, Palladium, and Silver". In: *Journal of Physical and Chemical Reference Data* 8.4 (Oct. 1979), pp. 1147–1298. ISSN: 0047-2689. DOI: 10.1063/1.555614.

- [45] Gaël Grissonnanche et al. “Linear-in Temperature Resistivity from an Isotropic Planckian Scattering Rate”. In: Nature 595.7869 (July 2021), pp. 667–672. ISSN: 1476-4687. DOI: 10.1038/s41586-021-03697-8.
- [46] S. Ghannadzadeh et al. “Simultaneous Loss of Interlayer Coherence and Long-Range Magnetism in Quasi-Two-Dimensional PdCrO<sub>2</sub>”. In: Nature Communications 8.1 (Apr. 2017), p. 15001. ISSN: 2041-1723. DOI: 10.1038/ncomms15001.
- [47] N. Kikugawa et al. “Interplanar Coupling-Dependent Magnetoresistivity in High-Purity Layered Metals”. In: Nature Communications 7.1 (Mar. 2016), p. 10903. ISSN: 2041-1723. DOI: 10.1038/ncomms10903.
- [48] Yawen Fang et al. “Fermi Surface Transformation at the Pseudogap Critical Point of a Cuprate Superconductor”. In: Nature Physics 18.5 (May 2022), pp. 558–564. ISSN: 1745-2481. DOI: 10.1038/s41567-022-01514-1.
- [49] Furrukh S Khan, John H Davies, and John W Wilkins. “Quantum transport equations for high electric fields”. In: Physical Review B 36.5 (1987), p. 2578.
- [50] FT Brandt, Renan Buosi Ferreira, and José Fernando Thuorst. “Classical Boltzmann equation and high-temperature QED”. In: Physical Review D 91.4 (2015), p. 045023.
- [51] Neil W. Ashcroft and N. David Mermin. Solid State Physics. Repr. South Melbourne: Brooks/Cole Thomson Learning, 2012. ISBN: 978-0-03-083993-1.
- [52] Hiroshi Takatsu and Yoshiteru Maeno. “Single Crystal Growth of the Metallic Triangular-Lattice Antiferromagnet PdCrO<sub>2</sub>”. In: Journal of Crystal Growth 312.23 (Nov. 2010), pp. 3461–3465. ISSN: 00220248. DOI: 10.1016/j.jcrysGro.2010.08.043.
- [53] E. C. Palm and T. P. Murphy. “Very Low Friction Rotator for Use at Low Temperatures and High Magnetic Fields”. In: Review of Scientific Instruments 70.1 (Jan. 1999), pp. 237–239. ISSN: 0034-6748. DOI: 10.1063/1.1149571.
- [54] Paul Goddard and Wadham College. “Magnetotransport Studies of Layered Metallic Systems”. In: () .
- [55] Wenjie Sun et al. “Title: Electronic Structure of Superconducting Infinite-Layer Lanthanum Nickelates”. In: () .
- [56] G Grissonnanche et al. “Electronic Band Structure of a Superconducting Nickelate Probed by the Seebeck Coefficient in the Disordered Limit”. In: () .

## A Extended Figures of the measurements at the NHMFL

Focusing on the results for  $\text{PdCoO}_2$ , sample D show extremely clean oscillations, to our recollection the cleaner than those seen in literature[47]. This is related to the fact that this is an extremely clean sample, with a residual resistivity of the order of the  $\text{m}\Omega$ . Sample C on the other hand, shows the same shape for every  $\phi$ , but as if it had been averaged. We attribute this to a higher elastic scattering in sample C, i.e., bigger amount of impurities. If this is true, we will be able to observe it directly from our calculations by simply increasing the  $T$ -independent elastic scattering rate. Therefore, both sets of curves are highly valuable, because they provide the same amount of information, they show reproducibility, and they will allow us to test our model for two different impurity densities. Another remarkable aspect from these curves is that the magnetoresistance barely decreases until  $\sim 60K^{10}$  (see the amplitude of the peaks) which is in line with the quasi plateau of resistivity seen in the normal resistivity (see Fig.3). This is also deeply related to the temperature evolution of the scattering rate in  $\text{PdCoO}_2$ , which from resistivity only kicks off above  $\sim 40\text{K}$ .

For  $\text{PdCrO}_2$  the story is quite different. We observe a display of small but well defined features that might even be mistaken by experimental noise. They are, however, completely reproducible, and are present in both samples as well. Sample A is the cleaner one in this case, and furthermore presents a higher symmetry along  $90^\circ$ . Sample B is quite asymmetric across such point, which is somewhat puzzling. In principle this asymmetry seems to be temperature independent, and hence should not have its origin in the Fermi surface folding across  $T_{\text{Neel}}$ . It is likely that the orientation of both samples was not perfect and therefore we are simply seeing two different regions of the Fermi surface, which again will be observable in our calculations. The most relevant observation of this data is that, in contrast to  $\text{PdCoO}_2$ , the ADMR oscillations are rapidly and completely washed out once we pass the AFM transition. This signifies a rapid increase of the scattering rate in the region immediately above the transition, region in which AFM fluctuations are prevalent and we start seeing strange metal behaviour.

---

<sup>10</sup>Indeed, they even seem to increase in sample C, although this may be effect of the applied normalization

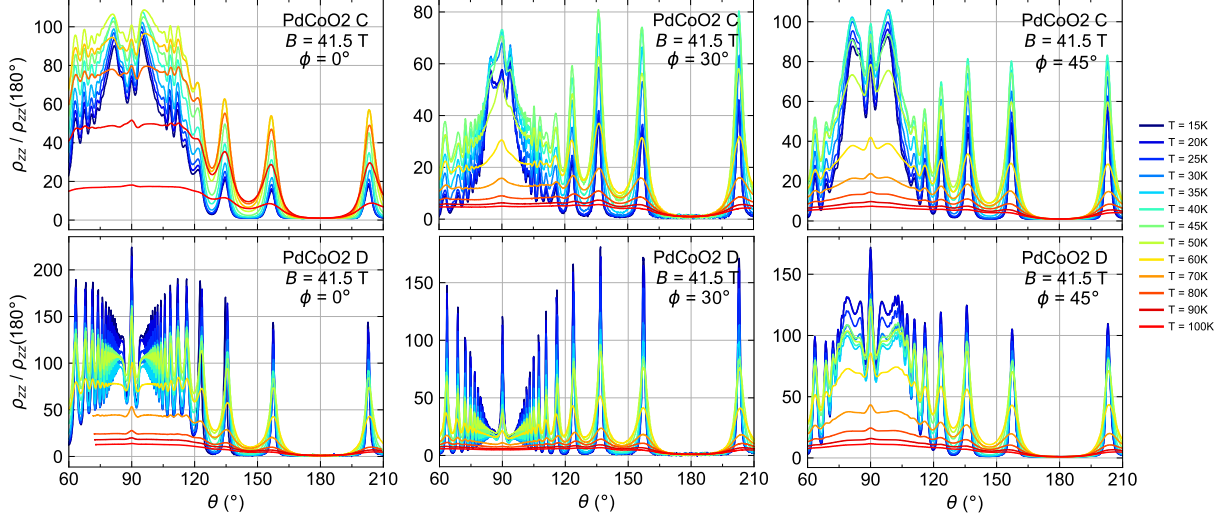


Figure S1: **Set of data for  $\text{PdCoO}_2$ .** At low temperature, the resistivity of  $\text{PdCoO}_2$  is almost constant (see Fig.3). This is observed in our data which shows almost no variation until 50K. Sample D is very clean, showing very prominent peaks at the Yamaji angles (see text), while sample C shows more disorder. This are good news, as in principle the only difference between both samples should be the elastic scattering rate caused by defects, which we can detect in our simulations.

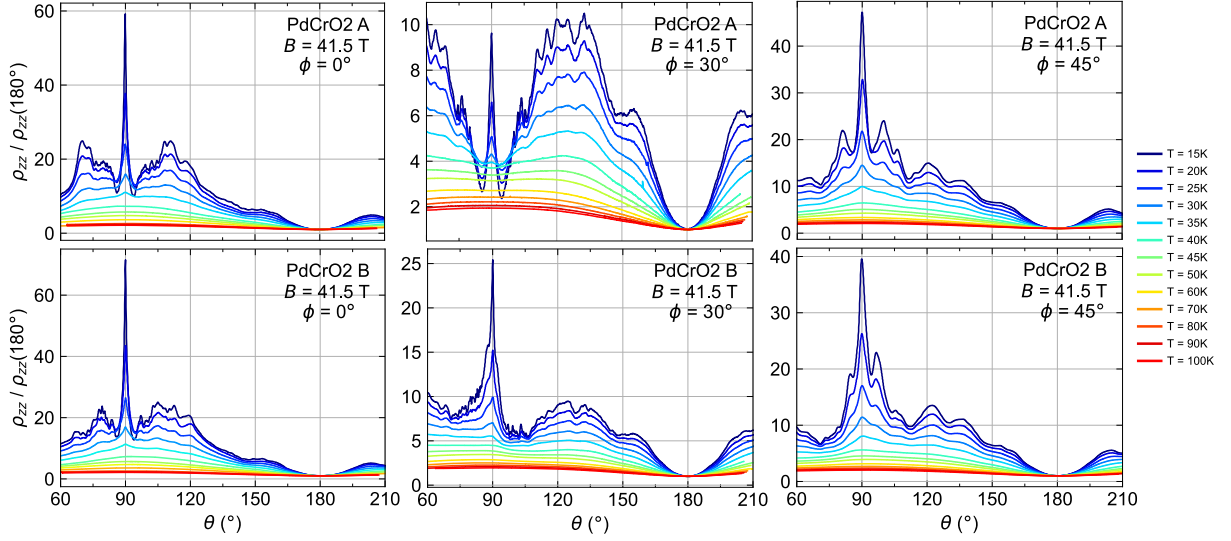


Figure S2: **Set of data for  $\text{PdCrO}_2$ .** The evolution with temperature is much more drastic than for  $\text{PdCoO}_2$ , once we go above the Néel transition of 37.5K. Sample B shows quite strong asymmetry across  $90^\circ$ , which may be related to the geometry of the Fermi surface. However, since neither sample A nor the  $\text{PdCoO}_2$  data shows this strength in asymmetry, we believe it is more related to misalignment of the  $\phi$  angle, which we will check with our simulations.

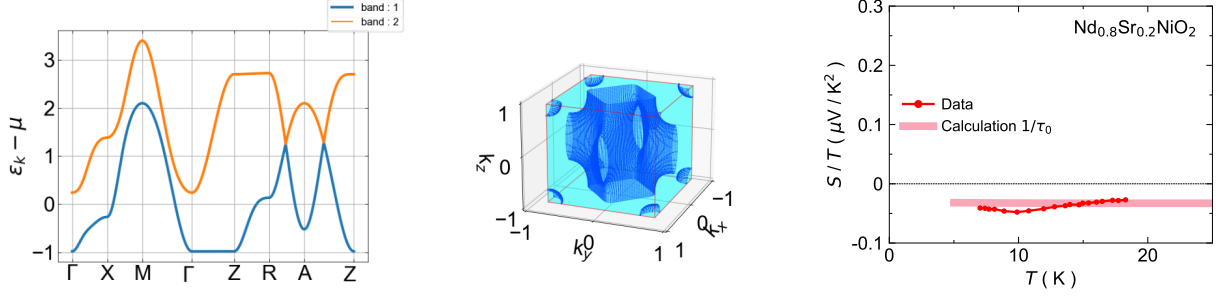


Figure S3: **Application of our code to LaNiO<sub>2</sub>.** (Left) Band structure. Band 1 denotes the band were all calculations will be made.(Center) Fermi surface calculated as the one for delafossites shown in Fig.10. It greatly resembles the Fermi surface presented in ref.[55].(Right) Seebeck calculation compared with the experimental value[56].

## B Simulations in Nickelates

As an example of the generality of our code, I present here an application to the case of infinite-layer nickelates. In Fig.S3, I show the band structure, which comes from diagonalizing the dispersion relation proposed in ref.[55], the calculated Fermi surface and the Seebeck coefficient as found with our code. The results are consistent with the observations[56].